DOI: 10.1002/ ((please add manuscript number))
Article type: Full paper

ZnO Coated Anodic 1D TiO_2 Nanotube Layers: Efficient Photo-electrochemical and Gas Sensing Heterojunction

*Siowwoon Ng, Petr Kuberský, Milos Krbal, Jan Prikryl, Viera Gärtnerová, Daniela Moravcová, Hanna Sopha, Raul Zazpe, Fong Kwong Yam, Aleš Jäger, Luděk Hromádko, Ludvík Beneš, Aleš Hamáček and Jan M. Macak**

((Optional Dedication))

S.W. Ng, Dr. M. Krbal, J. Prikryl, Dr. H. Sopha, Dr. R. Zazpe, L. Hromádko, Dr. J. M. Macak
Center of Materials and Nanotechnologies, Faculty of Chemical Technology, University of Pardubice, Nam. Cs. Legii 565, 53002 Pardubice, Czech Republic.
E-mail: jan.macak@upce.cz

S.W. Ng, Dr. F.K. Yam
School of Physics, Universiti Sains Malaysia, 11800 Penang, Malaysia.

Dr. P. Kuberský, Dr. D. Moravcová, Dr. A. Hamáček
Department of Technologies and Measurement/Regional Innovation Centre for Electrical Engineering (RICE), Faculty of Electrical Engineering, University of West Bohemia, Univerzitni 8, 30614 Plzen, Czech Republic.

Dr. V.Gärtnerová, Dr. A. Jäger
Laboratory of Nanostructures and Nanomaterials, Institute of Physics of the CAS, v.v.i., Na Slovance 2, 182 21 Prague 8, Czech Republic

Dr. L. Beneš
Joint Laboratory of Solid-State Chemistry, Faculty of Chemical Technology, University of Pardubice, Studentska 95, 532 10 Pardubice, Czech Republic

Keywords: self-organized TiO_2 nanotubes, ZnO coatings, ALD, charge separation, ethanol sensing

We demonstrate in this work a fascinating synergism of a high surface area heterojunction between TiO_2 in the form of ordered 1D anodic nanotube layers of a high aspect ratio and ZnO coatings of different thicknesses, produced by atomic layer deposition. The ZnO coatings effectively passivate the defects within the TiO_2 nanotube walls and significantly improve their charge carrier separation. Upon the ultraviolet and visible light irradiation, an increase of the ZnO coating thickness from 0.19 to 19 nm and an increase of the external

potential from 0.4 - 2 V, yields up to 8-fold enhancement of the photocurrent density. This enhancement translates into extremely high incident photon to current conversion efficiency of ~95 %, which is among the highest values reported in the literature for TiO_2 based nanostructures. In addition, the photoactive region is expanded to a broader range close to the visible spectral region, compared to the uncoated nanotube layers. Synergistic effect arising from ZnO coated TiO_2 nanotube layers also yields an improved ethanol sensing response, almost 11-fold compared to the uncoated nanotube layers. The design of the high-area 1D heterojunction presented here opens pathways for the light- and gas-assisted applications in photocatalysis, water splitting, sensors, and so on.

1. Introduction

Self-organized anodic titanium dioxide (TiO_2) nanotube layers present a fascinating, highly-ordered structure which has been extensively studied for more than a decade. Such structure is obtained through a well-developed electrochemical anodization of titanium metal.[1–4] The nanotube layers have been thoroughly investigated for their morphology, crystallinity and other properties for different applications.[5,6] Presently, TiO_2 nanotube layers have emerged as a promising material for photovoltaics,[7,8] photocatalysis,[9,10] chemical sensing[11,12] and biomedical applications.[13,14]

TiO_2 is an abundant, inexpensive, non-toxic and chemically stable compound but its major drawbacks are its low conductivity and high carrier recombination rate. Many efforts have been devoted to incorporate another material within the TiO_2 nanostructures (e.g. nanotube layers, mesoporous networks, nanorods and nanofibers). Metal oxides nanostructures (for example composed of WO_3,[15] SnO_2,[16] CuO,[17] NiO,[18] Al_2O_3,[19] In_2O_3,[20] and ZnO,[21,22]) turn out to be very suitable to form p-n or n-n junctions at the interface with TiO_2 to alter the band structure. Out of these, zinc oxide (ZnO) offers high electron mobility for fast charge transport and low carrier recombination rate. Apart from the

differences in conductivity and carrier recombination, it is also worth mentioning that ZnO and TiO_2 have close band gap energies (3.37 and 3.0-3.2 eV, respectively).[23,24] Since both materials complement in properties, many works have coupled ZnO and TiO_2 to form a new heterostructure, TiO_2/ZnO[21,22,25,26] or in a reverse manner, ZnO/TiO_2 structures.[27–29]

The advantages of ZnO-TiO_2 heterostructures include the suitable energy level alignment between ZnO and TiO_2, suppression of unwanted electron-hole recombination, shift in band gap energy, and hence extension of operational range in the visible spectral region.[26,27,30] These effects have been efficiently utilized for a high photocatalytic activity such as photodegradation of organic dyes[27–34] and H_2 production.[25] For example, in comparison with bare TiO_2 nanotubes, the ZnO-TiO_2 heterostructure recorded up to ~6.8 times more photocatalytic H_2 production.[25] As for efficient light conversion dye-sensitized solar cells (DSSCs), few angstroms thick ZnO sheath on TiO_2 nanowires has passivated the surface defect states on TiO_2.[22] Furthermore, ZnO coated TiO_2 nanotube layers presented 1.6 times photocurrent transient under visible light irradiation.[21] Under the shield of TiO_2, ZnO core-TiO_2 shell structures are also more resistant to photocorrosion.[27,30]

Advantages of the TiO_2/ZnO heterostructure can also be exploited for chemical sensing applications. As shown for brush-like ZnO-TiO_2 nanofibers,[35] TiO_2 core/ZnO shell nanorods[36] and TiO_2/ZnO double layer hollow fibers[37] heterostructures, an improved sensing performance can be associated with band bending due to Fermi level equilibration, reaction sites enhancement and synergistic reactions effect.[35–37] Moreover, the sensitivity is maximized if the sensing layer is fully depleted, that is, if the nanostructure dimension is comparable to the electron depletion layer. TiO_2 core/ZnO shell nanorods have shown enhanced sensing sensitivity up to ~5 times compared to the pristine TiO_2 for ethanol detection due to enhanced adsorption and desorption of ethanol, as well as due to the surface depletion effect.[36]

There are numerous approaches to integrate ZnO within TiO_2 nanostructures, such as chemical bath deposition,[25] dip-coating,[26] sputtering,[29] hydrothermal,[35] layer-by-layer assembly[38] and atomic layer deposition (ALD).[21,22] However, only ALD produces conformal and homogeneous deposition of a thin layer of material, with precise control of the coating thickness according to the deposition cycles.[39] The peculiar characteristics are particularly helpful for the deposition of a secondary material in high aspect ratio structures, such as porous anodic alumina, and TiO_2 nanotube layers, as in this study. Very recently, a few works have shown the potential of ALD secondary material in TiO_2 nanostructures.[21,22,34,36,37,40–45] These include ALD ZnO loaded TiO_2 nanowires and nanotubes, both focused on the photocatalytic and photoelectrochemcial (PEC) applications.[21,22,34,40] However, gas sensing application based on ALD prepared TiO_2/ZnO heterostructure are limited. Up to now, hydrothermally grown TiO_2 nanorods with ALD ZnO shell have been applied for detection of low concentration ethanol at 150 ^oC,[36] and ALD double-layer TiO_2/ZnO hollow fibers for improved detection of CO gas.[37] Nevertheless, the reported well-aligned or highly ordered TiO_2 core nanostructures were in thicknesses 0.5-2.3 µm,[21,22,34,36,40] which possessed limited surface area for light induced photoactivity and efficient sensing. Thus, it is beneficial to explore uniform ZnO coatings from surface to bottom of higher aspect ratio TiO_2 nanotubes layer.

In this work, we deposited ZnO coatings of different thicknesses from 0.19 to 19 nm within ~5 µm thick self-organized anodic TiO_2 nanotube layers with inner diameters ~230 nm, equivalent to aspect ratio ~22. The preparation of this heterostructure is illustrated in **Figure 1**. We evaluated the performance of the ZnO coated TiO_2 nanotube layers from two different aspects, i) the photocurrent generation as a function of an externally applied potential and ii) the ethanol sensing response at low temperatures.

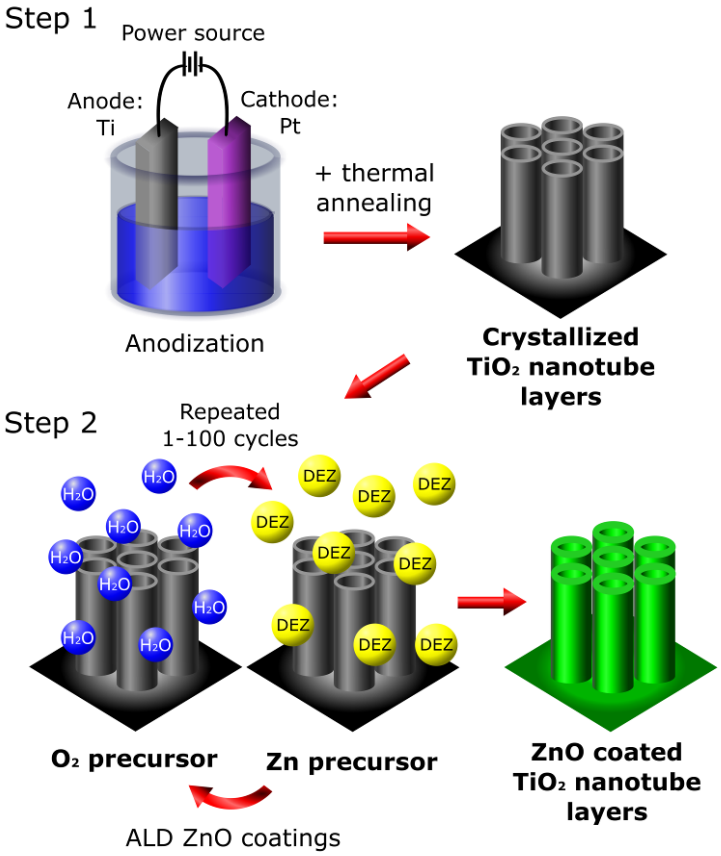

Figure 1. Schematic illustration of the preparation of ZnO coated TiO_2 nanotube layers.

2. Results and Discussion

2.1. Morphology and Structural Properties

Self-organized TiO_2 nanotube layers with thickness of ~5 µm and inner diameter ~230 nm were prepared according to the well-established recipe[46] and further used for ALD coatings of ZnO. Illustrative scanning electron microscope (SEM) images of the uncoated nanotube TiO_2 layer are provided as a reference in **Figure S1** (Supporting Information). **Figure 2**a presents the SEM image of the ZnO (19 nm) coated TiO_2 nanotube layers. The wall thickness of the blank TiO_2 nanotube layer and the thickness of ZnO ALD coating (19 nm) measured at top, middle and bottom of the tube layers are summarized in **Table S1** (Supporting Information). The coating thickness measured from SEM images of ZnO coated TiO_2 nanotube layers well agrees with the thickness separately evaluated from ellipsometric

measurement carried out on identical ALD ZnO coating on Si wafer. It is evident that during the ALD process, the ZnO is deposited on any exposed surface of TiO_2 nanotube layers, and follows the tubular topography. In the magnified view in Figure 2b, the entire inner and outer walls of the tubes are uniformly covered by ZnO, visible due to different mass contrast between the two materials. The observation is supported by the scanning transmission electron microscopy-high angle annular dark field (STEM-HAADF) image in Figure 2c and its enlarged view in Figure 2d. Both images show two distinct tube walls, and the white ZnO layer completely enfolds the tubes. Similarly, homogeneous coatings were achieved within our previous works on Al_2O_3 coatings for thermal stability and Li-ion batteries,[41–43] TiO_2 coatings for photocatalysis,[44] and CdS coatings for solar cells,[45] respectively, within anodic TiO_2 nanotube layers. Figure 2e,f show the selected area electron diffraction (SAED) and XRD patterns of the ZnO (19 nm) coatings within TiO_2 nanotube layers, respectively. The clearly seen SAED diffraction rings reveal that both ZnO coatings and TiO_2 nanotube layers possess polycrystalline structure. Individual crystallographic planes were indicated in Figure 2e and are in complete match with the XRD pattern in Figure 2f. In accordance with our expectation, the anodic TiO_2 nanotube layers annealed at 400 ^oC yield polycrystalline anatase structure, with (101) dominant plane in both patterns. On the other hand, the ZnO layers are readily crystallized during the ALD process (200 ^oC) and the signature reflections are shown in both patterns as well. This observation well agrees with Rogé *et al.* [47] who employed similar ALD precursors and deposition conditions for ZnO layers.

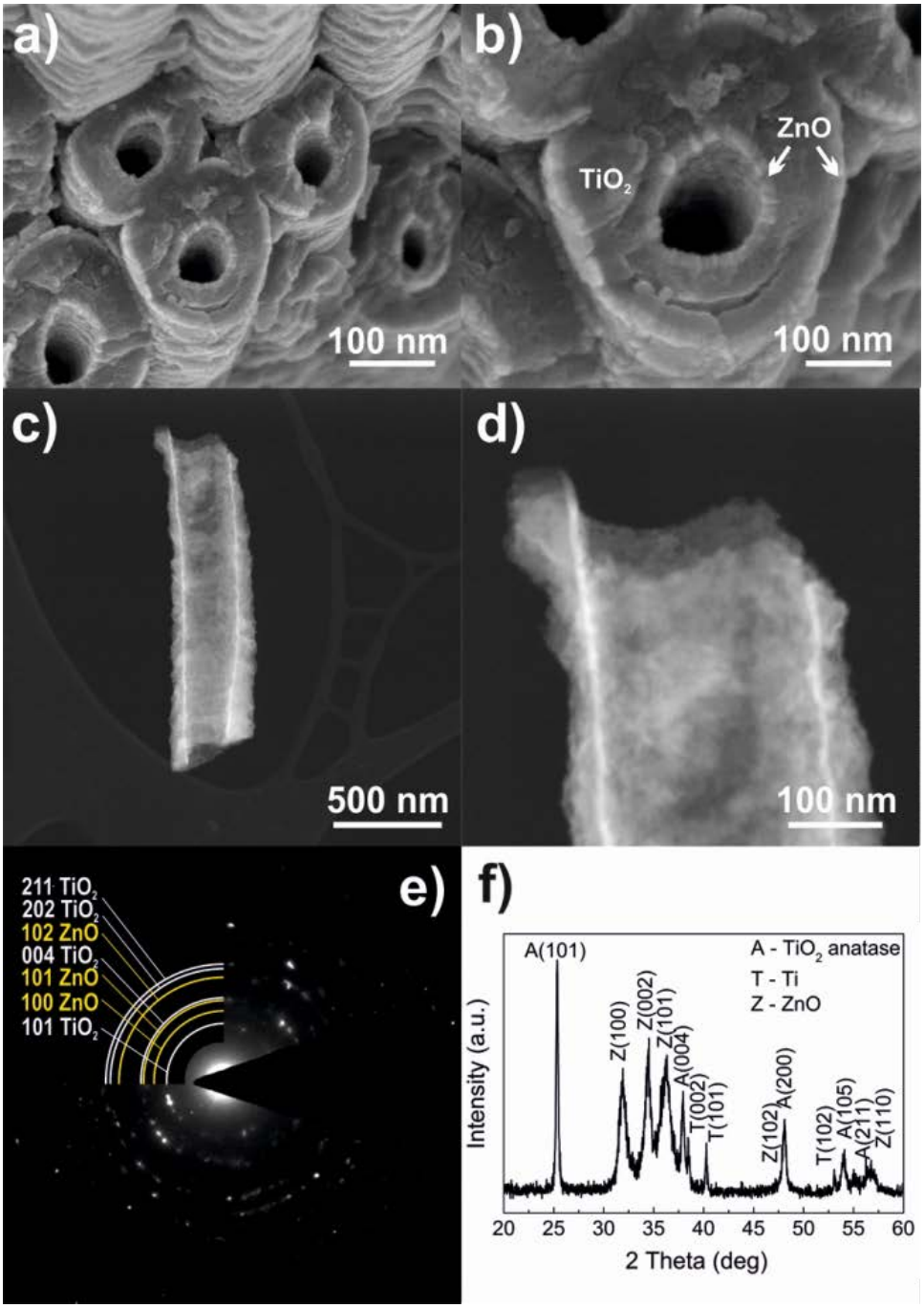

Figure 2. Morphology and structural properties of ZnO coated TiO_2 nanotube layers. (a)-(b) SEM and (c)-(d) STEM-HAADF images, (e) SAED pattern with indicated crystallographic planes (evaluated from d-spacings) and (f) XRD pattern, of the same ZnO coated (19 nm) TiO_2 nanotube layer.

2.2 Photoelectrochemical (PEC) activity Following the uniform deposition of ZnO coatings within TiO_2 nanotube layers, we investigated the PEC activity of this hybrid structure. **Figure**

3a-d shows the photocurrent densities and incident photon-to-electron conversion efficiencies (IPCE) of the blank TiO_2 nanotubes and the ZnO coated (19 nm) TiO_2 nanotube layers, recorded at different potentials against the Ag/AgCl reference electrode, i.e. 0.4 - 2 V. For blank TiO_2 nanotube layers, the applied potential also enhances the charge separation, but the photocurrent reaches its saturation due to the depletion of the space charge layer. This is apparent from the nearly identical values in Figure 3a, and in accordance with the previous literature[32]. In other words, the space charge layer formed at applied potentials higher than 0.2 V is saturated when the space charge layer thickness is close to the nanotube wall thickness, applied in this work.[48,49]

In contrast, for ZnO coated TiO_2 nanotube layers, a remarkable enhancement in photocurrent density and IPCE was observed with increased potentials, as illustrated in Figure 3c,d. Overall, for each step-up of 0.4 V in the range 0.8 - 2 V, a uniform increment in photocurrent was revealed, up to ~120 µA cm^{-2} with a corresponding enhancement factor of ~4 - 8. In addition, the IPCE values reached ~95 % at wavelengths between 350 - 375 nm, and more than 80 % for 250 - 350 nm. These values clearly show that the applied potential effectively facilitates the separation of photogenerated electrons and holes within the ZnO coated TiO_2 nanotube layers due to the band bending effect, in addition to the charge separation within each single material. Although ZnO-TiO_2 combination among various hetero-nanostructures has been reported for enhanced PEC activity, in this work, the ALD ZnO coatings within TiO_2 nanotube layers promoted the photocurrent conversion efficiency close to 95 %, which is among the highest reported values to the best of our knowledge. For comparison, identical ALD ZnO coatings were deposited within ~5 µm TiO_2 mesoporous layers to perform the same photocurrent measurements. The 19 nm ZnO coated TiO_2 mesoporous layer achieved its highest photocurrent density at ~7 µA cm^{-2} as shown in **Figure S2** (Supporting Information) for reference. These values have shown strong improvement compared to the blank TiO_2 mesoporous layer, but incomparable to the ZnO coatings within

the TiO_2 nanotube layers. Based on these results, we are convinced that the high photocurrent densities and IPCE values stem from the mutual contribution from the TiO_2 nanotube layer and the additional ZnO coatings.

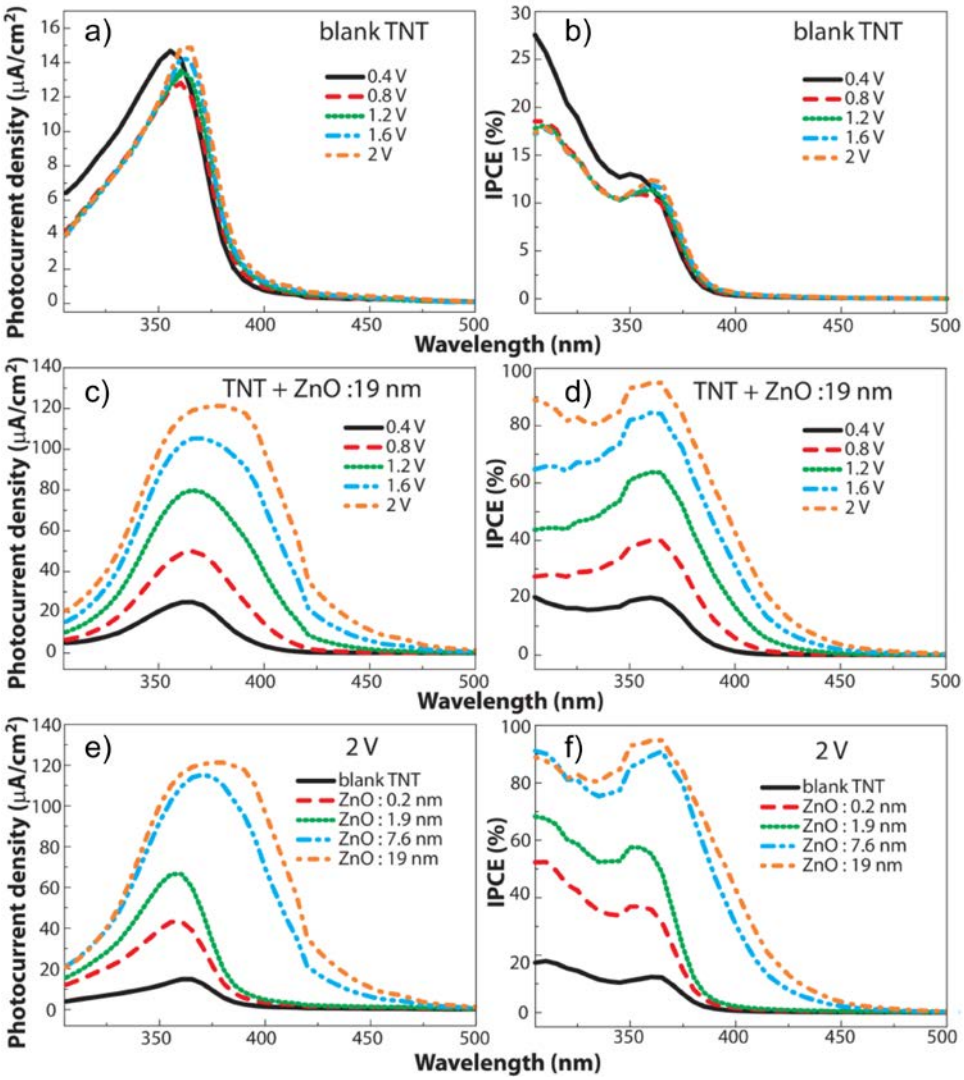

Figure 3. Photocurrent densities (left column) and IPCE values (right column). Measurements were carried out in the potential range of 0.4 - 2 V for (a, b) the blank anodic TiO_2 nanotube layer, (c, d) ZnO coated (19 nm) TiO_2 nanotube layer, (e, f) blank and ZnO coated (0.19, 1.9, 7.6 and 19 nm) TiO_2 nanotube layers at 2 V.

The PEC activity was also investigated for ALD ZnO coatings with various thicknesses. The results are displayed in Figure 3e,f, a significant increase in PEC activity can be seen with the increased ZnO coating thickness. The 0.19 and 1.9 nm ZnO coatings in this

work have revealed photocurrent density improvements of ~2.5 - 4.5 times compared to that of the blank TiO_2 nanotube layer under 2 V. Up to 50 % IPCE value in the UV range is attained already by 1 cycle addition of ZnO coating (corresponds to 0.19 nm) within the TiO_2 nanotube layers, as a result of the surface state passivation which improves the charge collection efficiency.[22] Several works reported that the highest photocurrents were obtained for TiO_2 nanostructures coated by 1-10 cycles (equivalent to sub-nm, or ≤ 2 nm thickness) of ALD ZnO coatings, and thicker coatings have shown a detrimental effect.[22,34,40] In contrary to these works, our results clearly indicate that the enhancement factor has raised to ~7 - 8 for subsequent increment of ZnO layer thickness to 7.6 and 19 nm. It is also interesting to note that the IPCE of 7.6 nm ZnO is very similar to the 19 nm, which suggests that the PEC enhancement effect by ZnO coatings has approached the saturation level.

Upon irradiation, the excitation of electrons occurred in both ZnO and TiO_2 layers, indicated by the arrows in **Figure 4**. The ZnO coatings (maximum thickness 19 nm) are too thin to completely shield the TiO_2 nanotube layers from absorbing the incident light, because in the UV (~340 nm) and visible (~500 nm) spectral region, the corresponding absorption depths are ~500 nm and ~50 μm, respectively.[50] In general, the significantly improved PEC activity of ZnO can be attributed to the TiO_2/ZnO heterojunction structure that promotes the separation of charge carriers and increases their lifetime.[40] The schematic diagram of energy levels in Figure 4a shows the staggered band formed between ZnO and TiO_2, in which the conduction band of ZnO is slightly higher than that of TiO_2, with work function of ZnO (5.2 - 5.3 eV) also slightly higher than anatase TiO_2 (~5.1 eV).[26] When an external potential is applied to the heterostructure, the electrons from the conduction band of ZnO will be transferred to the conduction band of TiO_2, whereas the holes in the valence band of TiO_2 will be channeled to the valence band of ZnO.[26] In the case of ZnO coated TiO_2 nanotube layers, two more aspects are needed to be considered. At first, the ultrathin coatings of ZnO passivate the surface traps of the TiO_2 nanotubes by filling the oxygen vacancy defects with an oxygen

containing molecule.[22,34] Thus, the reconstructed tube walls suppress the charge carrier recombination and efficiently convert the photons to electrons. This is in line with our previous work on ALD TiO_2 coatings within TiO_2 nanotube layers.[44] Secondly, at the electrolyte and ZnO coatings interface, the electrons are efficiently transported through the nanotube layers and then to the metallic Ti substrates present underneath. In fact, upon the UV irradiation, the depletion width is decreased as a result of increased ZnO charge carrier density. This is because oxygen is adsorbed on the surface of ZnO layer (n-type, intrinsic, with excess electrons) to form oxygen species (O_2^-), and the oxygen vacancies of ZnO are related to deep level trapping.[51] The holes are then captured by the negatively charged oxygen ions to form oxygen again.[52] The reduced depletion width and the applied potential both enable higher migration rate of electrons across the energy barrier at the interface of both oxides. As a result, higher applied voltages increasingly contributed to the generation of more photoelectrons and increased photocurrent densities (as shown in Figure 3).

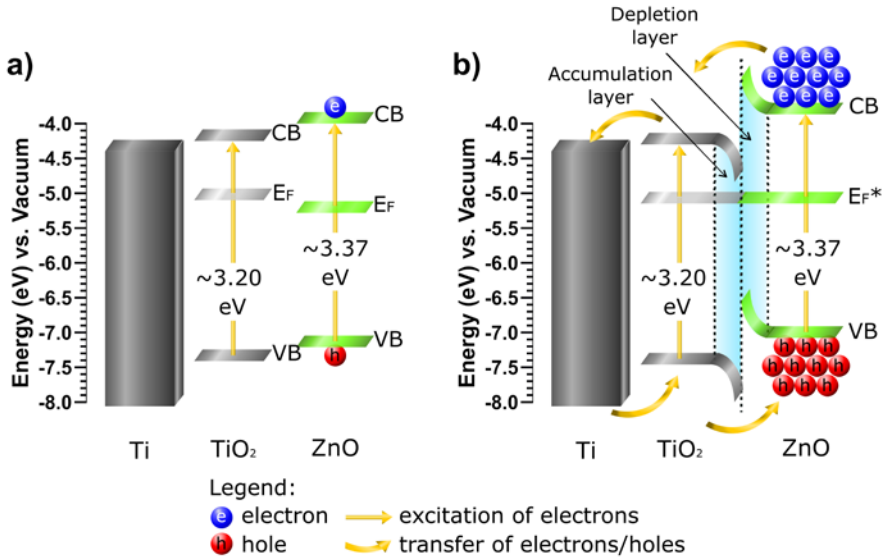

Figure 4. Schematic diagram of the energy levels of ZnO coated TiO_2 nanotube layers grown on Ti substrates. (a) Before and (b) after Fermi level alignment. E_F* shows aligned Fermi level at an approximate position, since the exact position is unknown. Excitation of electrons from valence band to conduction band for TiO_2 and ZnO, and charge transport across the ZnO/TiO_2/Ti interfaces and reverse directions are shown.

In comparison to the photocurrent densities and IPCE for blank TiO_2 nanotube layers, the ZnO coated TiO_2 nanotube layers have a broader photoactive region, falling within the visible spectral region. It means that the optical band gap of resulting TiO_2–ZnO heterostructure is reduced when sufficient amount of ZnO coatings is loaded within the TiO_2 nanotube layers, in combination with an externally applied potential. Under an external potential ≥ 1.6 V (refer Figure 3c), the original maximum photocurrent density at 360 nm for TiO_2 nanotube layers shifts to 375 nm for 19 nm thick ZnO coated nanotube layers, and the photocurrent density is tailing up to ~425 nm. For lower ZnO thicknesses (below 7.6 nm, refer Figure 3e), even though the generated photocurrent density is higher compared to the blank nanotube layers, the active region is rather narrow, and the photocurrent density peaks at 360 nm. With increasing thickness of ZnO coatings (7.6 nm and more), the photoactive region is pronouncedly expanded to 425 nm and the peak of photocurrent density is situated at 375 nm.

To investigate the peak shift and enhanced PEC response in the visible spectral region, diffuse reflectance measurement was carried out and shown in **Figure 5**a. With reference to the blank TiO_2 nanotube layer, red shift from ~400 to ~450 nm, as well as decrease in reflectance from maximum 26 % to 17 % were observed for increased ZnO coating thickness. The lower diffuse reflectance suggests that the adequately coated walls are smoother than the walls of the uncoated tubes, resulting in stronger light absorption over the visible spectral region. Similar effects have been achieved by ALD In_2O_3 coated TiO_2 nanotube layers.[20] Figure 5b presents the corresponding optical band gaps evaluated from Tauc plot in combination with Kubelka-Munk function, using indirect allowed transition for anatase TiO_2. The bandgap energy determined from the extrapolation of the linear portion of the plots to the energy axis shows that the blank TiO_2 nanotube layer possesses optical band gap energy of 3.07 eV and gradually decreases to 2.98 and 2.76 eV with added ZnO layer thicknesses 7.6

and 19 nm, respectively. A noticeable red shift of the reflectance edge in the ZnO coated layers which occurs as a result of mixed crystals of ZnO and TiO_2 (proven by SAED and XRD measurements). The bandgap energy of any crystalline semiconductor is partially influenced by the crystallinity of a film.[53] Therefore, the coated ZnO layer has good crystallinity, demonstrated by strong XRD signal for 19 nm ZnO. In addition, the difference in surface states increases the photogenerated charge separation and extends the photoexcited region to visible spectral range. This is only possible with the co-existence of ZnO, therefore the increased coatings of ZnO further extend the red shift, i.e. decrease in the optical bandgap. Overall, the reflectance measurement and band gap evaluation substantiate the escalated photoactivity in Figure 3 for the ZnO-TiO_2 heterostructure, particularly the 19 nm thick ZnO.

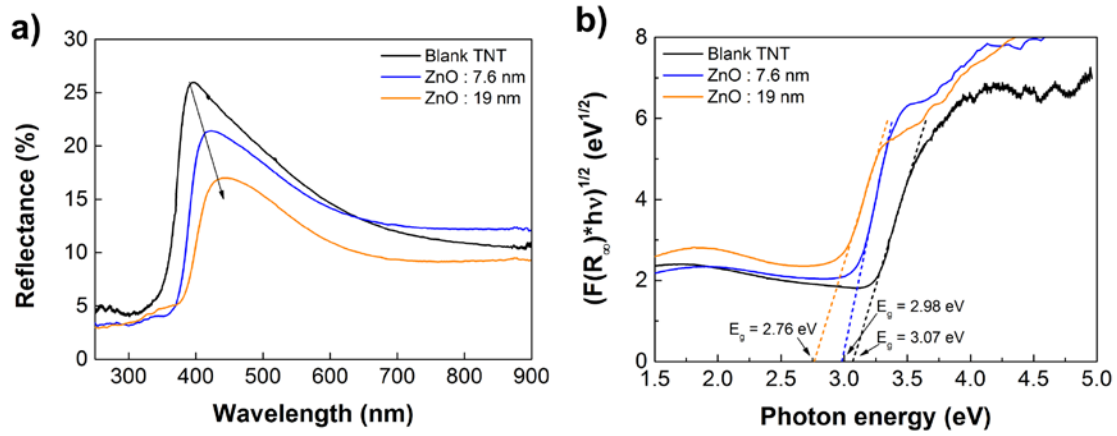

Figure 5. (a) Diffuse reflectance measurement and (b) Tauc plot of the Kubelka-Munk function, for blank and ZnO coated (7.6 and 19 nm) TiO_2 nanotube layers.

2.3 Ethanol sensing response As extensive research in the literature has been focused on the role of ZnO in light-driven applications, it is also interesting to investigate the possibility to apply the ZnO-TiO_2 heterostructure in gas sensing, which is another crucial application for metal oxides semiconductor. **Figure 6** presents the sensing response and recovery given by the ratio of the initial electrical resistance in air to the electrical resistance when ethanol vapor was applied, R_O/R_g as a function of time, towards 1930 ppm ethanol tested at 100 and 200 ^oC.

When ethanol vapor was introduced into the test chamber, a change in resistance was observed for all samples. A decrease in resistance upon exposure to ethanol indicates that the presented ZnO-TiO_2 heterostructure adopts the n-type semiconductor behavior of their individual constituents. When the ethanol was removed from the chamber by purging synthetic air, the resistance of the layers increased and resembled nearly its initial value. Similar to the PEC activity, with reference to the blank TiO_2 nanotube layers, layers with thicker ZnO coatings have shown stronger improvement for ethanol sensing response. For sensing response measured at 100 ^{o}C, a minor enhancement was observed for 0.19 nm thick ZnO and a double enhancement was credited to 1.9 nm thick ZnO coatings. Subsequently, with 7.6 and 19 nm thick ZnO coatings in the nanotube layers, a dramatic improvement in the response of ~6 - 8 times were recorded. In addition, for blank and 0.19 nm ZnO coated tubes, the change of resistance was slow and approached saturation after some time. As for thicker ZnO coatings within TiO_2 nanotube layers, the resistance continued to decrease without saturation sign with the continuous supply of ethanol. As a sensing response is highly dependent on the operating temperature, we proceed to examine the response at 200 ^{o}C. Again, a tiny enhancement was observed for 0.19 nm thick ZnO coated TiO_2 nanotube layer with reference to the blank nanotube layer. In ascendance, 1.9, 7.6 and 19 nm thick ZnO coatings have demonstrated outstanding improvement by ~4, 5 and >11 times, respectively. Between two working temperatures, thick ZnO coatings have shown much improved sensitivity and shorter response time at 200 ^{o}C, as compared to the same coating thicknesses at 100 ^{o}C. Furthermore, the response and recovery time upon exposure and removal of ethanol vapor were shorter for ZnO coatings ≥1.9 nm, and the change in resistance was inclined towards saturation after a shorter time.

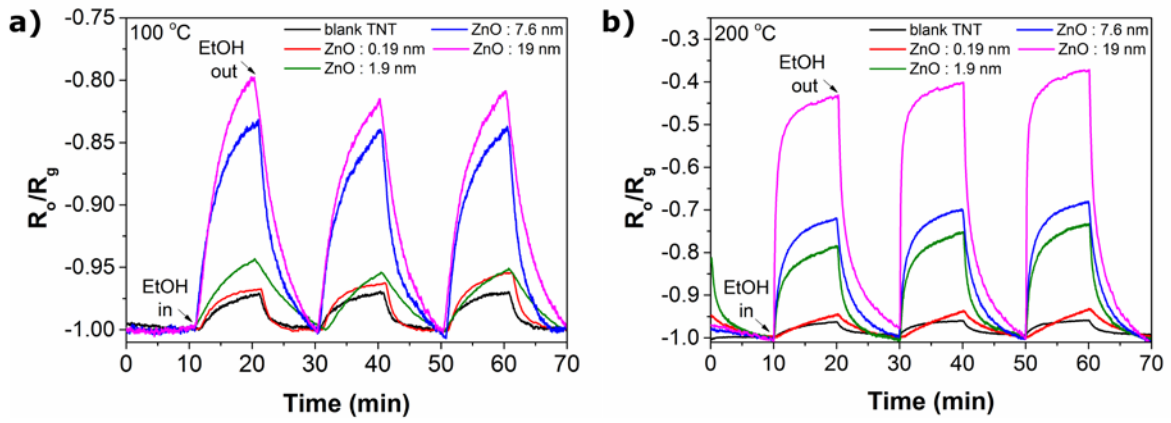

Figure 6. Sensing responses for 1930 ppm ethanol at 100 °C (a) and 200 °C (b)**.** The response is expressed in the ratio of R_O/R_g for blank and ZnO coated (0.19, 1.9, 7.6 and 19 nm thick) TiO_2 nanotube layers.

ZnO (19 nm) coated TiO_2 nanotube layer was further explored for its sensing response, repeatability and stability. **Figure 7**a presents its different responsive behavior at two sensing temperatures. As discussed earlier, at 200 °C, the shark-fin behavior was flattened and more prone to saturation. This implies that the ZnO coated TiO_2 nanotube layer rapidly responded to the ethanol gas and the sensitivity was enhanced 3 times compared to that at 100 °C. Figure 7b shows that the sensing response also changed with changing ethanol concentrations, when the layer was continuously exposed to different ethanol concentrations from 480 to 1170 ppm. The layer was capable of detecting a smaller amount of ethanol at 480 ppm, and for the subsequent increment from 810 to 1170 ppm, the increment in response was almost linear. When ethanol concentration was reduced, the response was reduced accordingly. This shows that the ZnO coated TiO_2 nanotube layer is sensitive towards the change of concentration, with an advantage to carry out calibration for detection of a range of ethanol concentrations. Lastly, the reproducibility for 1170 ppm ethanol at 200 °C was tested, as shown in Figure 7c,d. A high stability and repeatability for continuous measurement over ten identical test cycles were demonstrated with almost no deterioration in response. The same layer has exhibited

excellent durability under long hour exposure to ethanol. We also note that for the case of 1170 ppm in Figure 7b-d, the maximum Ro/Rg ratio is consistently 0.7±0.05. These observations support the ZnO coated TiO_2 nanotube layer to be a robust and stable gas sensor.

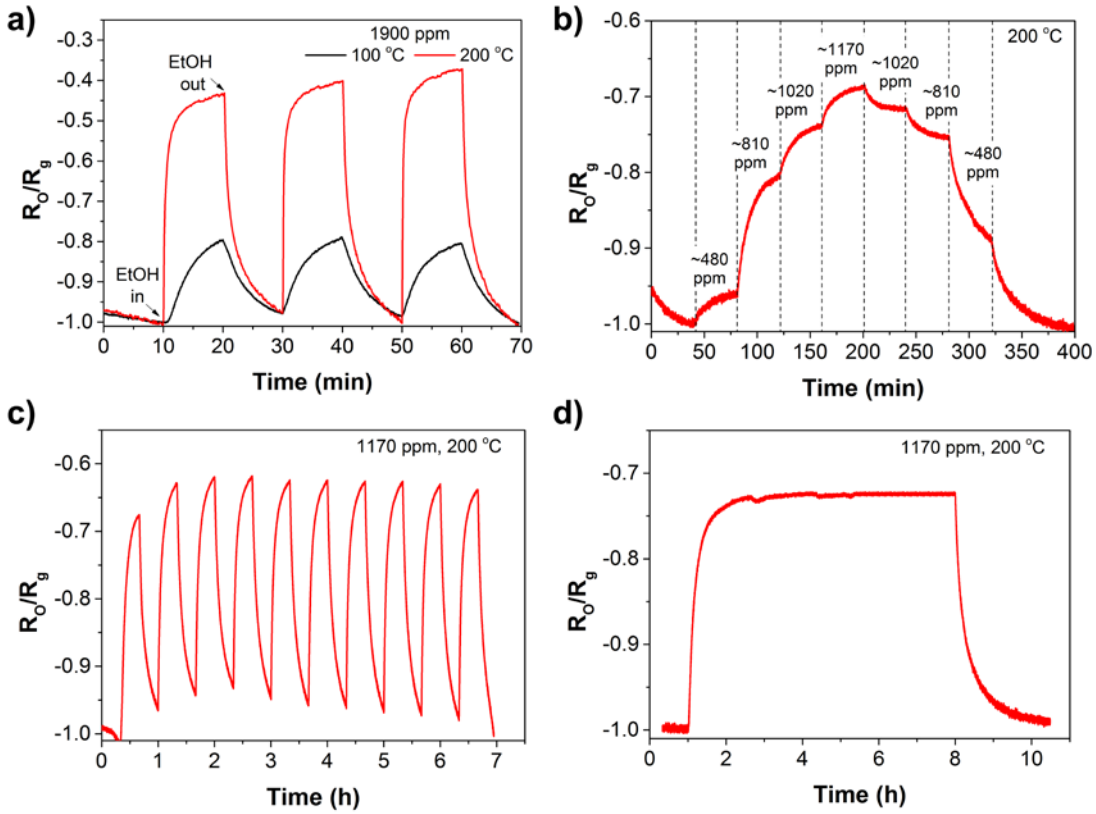

Figure 7. Ethanol sensing response of ZnO (19 nm) coated TiO_2 nanotube layer tested in different conditions. (a) Operating temperature of 100 and 200 ^oC, (b) exposure to different ethanol vapor concentrations from ~480 to 1170 ppm, (c, d) reproducibility and stability test over many cycles and long hours, respectively.

In order to discuss the sensing response of the presented heterostructures, one has to keep in mind that the operation of metal oxide semiconductor gas sensors is usually based on the alteration of its electrical resistance upon exposure to a targeted gas. The change of resistance occurs, when there is an interaction between active species on the structure surface and the gas molecules. The sensing mechanism of the ZnO coated TiO_2 nanotube layers follows the surface depletion model.[54–56] Under an atmospheric ambient, the initial resistance

of the ZnO coated TiO_2 nanotube layers is high because the oxygen molecules are adsorbed on the structure surface and form chemisorbed oxygen species (O_2^- for <150 ^oC; O^- and O^{2-} for ≥150 ^oC) by capturing electrons from the conduction band.[16,36,57]

The adsorbed oxygen species then deplete the surface electron states and reduce the carrier concentration, hence create a surface charge depletion layer at the surface of ZnO. When the samples are exposed to ethanol vapor, reactions occur between the ethanol molecules and adsorbed oxygen species. The trapped electrons are transferred from ethanol to the sensor by the adsorbed oxygen species, which serves as an electron bridge. As a result, the electrons are released back to the conduction band, resulting in an increase in carrier concentration, decrease in depletion width and hence the overall resistance is decreased.[36,58,59]

Similar to the enhancement of PEC activity, the improvement in sensing response of TiO_2 nanotube layers with increased thickness of ZnO coatings again can be ascribed to two major factors, one from the heterojunction effect, and the other from the ZnO coatings.

Firstly, at the interface between the ZnO and TiO_2, an n-n heterojunction is formed as shown in Figure 4a. The work function of ZnO is higher than that of TiO_2, thus, electrons from the conduction band of ZnO are transferred to TiO_2.[35] The migration of electrons to align the two Fermi levels resulting in an energy barrier, which creates depletion and accumulation layers at the interface, causes the band bending between ZnO and TiO_2,[16,57] shown in Figure 4b. The adsorption of oxygen (discussed earlier) and formation of negatively charged ions results in upward bending of ZnO. When the adsorbed oxygen species react with ethanol and release electrons, the energy barrier is decreased. The resistance of the heterojunction, R, is proportional to the energy barrier, $q\phi$, in equation (1):

$$R \approx \exp [(q\phi)/kT] \qquad (1)$$

where k is the Boltzmann constant and T is the temperature. The decrease in heterojunction energy barrier narrows the depletion and accumulation layer width. Under such condition, the

electrons are able to cross the energy barrier to the accumulation region in TiO_2. Moreover, the applied potential further drives the electrons from the accumulation region of TiO_2 towards Ti, resulting in a huge increase in the overall conductivity. Upon removal of ethanol, the increase in energy barrier height widens the depletion region, hence the electrons are confined and increased resistance is recorded. In addition, the heterojunction serves as additional active sites for ethanol adsorption as well as the reaction of ethanol with surface-adsorbed oxygen ions for improved sensing responses.[57]

As blank TiO_2 contains more oxygen defects than ZnO, it has a stronger oxygen adsorption.[60] For acidic metal oxide TiO_2, dehydration of ethanol is the dominant process with limited dehydrogenation activity, whereas ZnO is an amphoteric metal oxide, known as better catalyst with higher dehydrogenation activity, which is preferable for sensing purpose.[59,61] Combined metal oxides usually demonstrate higher activity and better selectivity than their single metal oxide counterparts.[61] Enhanced response towards ethanol has been achieved through integrating two metal oxides, e.g. for SnO_2-ZnO, SnO_2-TiO_2, CuO-ZnO, and WO_3-ZnO structures.[16,62–64] Similarly, for the ZnO and TiO_2 heterostructure, adsorption of rich oxygen species and synergistic catalytic breakdown of ethanol occurred,[64] specifically when sufficiently thick ZnO coatings were added to TiO_2 nanotube layers, i.e. 7.6 and 19 nm in thickness. Even these thickest coatings in this work did not inhibit the TiO_2 nanotubes layer underneath from adsorbing ethanol and participating in the sensing reaction. Park *et al.* reported 15 nm ZnO coatings on TiO_2 nanorods[36] whereas Tharsika *et al.* utilized 20 nm ZnO coating on SnO_2 nanowires,[65] both core and shell layers worked perfectly well for ethanol detection.

For the ZnO coatings, such layers provide more active sites for ethanol adsorption and desorption, which increase the reaction rate between ethanol and surface oxygen species.[66] Based on Figure 7a, it is evident that the sensing response curve of the blank and ZnO (0.19 nm) coated TiO_2 nanotube layers approaches saturation after a certain period. For thicker

ZnO coatings, the response curves feature a shark-fin behavior with no trace of saturation after 10 min of exposure to ethanol. This implies that the sensors offer more active reaction sites and adsorbed oxygen species to capture more electrons from ethanol. Due to the unsaturated reaction sites, shorter response and recovery time are registered for the ZnO coated TiO_2 nanotube layers, compared to the blank nanotube layers.[64]

This deduction is substantiated by the sensing response at 200 ^{o}C (Figure 7b), where the available active reaction sites of the heterostructure are more readily utilized for the interactions with electrons from ethanol, which rendered saturation response. Moreover, elevated sensing temperature initiates higher dehydrogenation rate of ethanol, and enables the formation of specific type of adsorbed oxygen species, i.e. O^- and O^{2-} to release the adsorbed electrons.[57] All in all, these factors intensify the sensitivity and reduce the response time at 200 ^{o}C.

In the earlier part, we discussed that the charge depletion layer is created at the ZnO outer surface by the oxygen species. For a nanotubular polycrystalline structure, the sensitivity is affected by the wall thickness of the structure. When such thickness is in the range of the electron depletion layer or Debye length, given in equation (2),[67] the sensitivity is maximized.[37,62]

$$L_D = \left[\frac{\varepsilon k_B T}{q^2 N_C} \right]^{\frac{1}{2}} \quad (2)$$

In equation (2) ε is the static dielectric constant of ZnO, q is the electron charge, N_c is the carrier concentration of ZnO, k_B is the Boltzmann's constant, T is the absolute temperature, and L_D is strongly dependent on the operation temperature and carrier concentration. Most of the reported gas sensing works were operating at temperatures above 250 ^{o}C and the Debye length was estimated to be 20 - 35 nm.[37,68] Therefore, we believe that for 100 - 200 ^{o}C, the Debye length is closer to the lower values in the estimation range.

In this case, ALD ZnO coated TiO_2 nanotube layers offer ultrathin coatings between 0.19 to 19 nm, which is smaller but close to the average estimated Debye length. Therefore, it is possible that the coatings created by ZnO grains for 7.6 and 19 nm thick coatings which are in the range of Debye length, are fully depleted and therefore show a tremendous improvement in the sensing response.

3. Conclusion

We reported on ALD thin ZnO coatings within anodic 1D TiO_2 nanotube layers with superior PEC activity and strongly enhanced ethanol sensing response. An improved performance was observed with the increase of ZnO coating thickness for both applications. In combination with externally applied potential, a more than 20 nm redshift in the photoresponse, closer to the visible spectral region was observed. For ZnO coated (19 nm) TiO_2 nanotube layers, up to 8-fold enhancement in photocurrent density, and IPCE of 80 - 95 % between 305 - 375 nm were obtained under an external potential of 2 V, which are the highest values ever reported. The ZnO coatings TiO_2 nanotube layers have demonstrated enhanced sensitivity for ethanol detection at low temperature. At 200 ^{o}C, 11-fold enhancement ethanol of sensing response was attained for 1930 ppm ethanol vapor. The additional ZnO coatings act as follows: i) provide more active sites for ethanol adsorption and desorption, ii) possess higher dehydrogenation activity than TiO_2, iii) enhance the sensing response due to their almost full depletion. As for the ZnO/TiO_2 hybrid structure, additional interface was formed at the heterojunction that i) facilitates the charge carrier separation and a smooth charge transfer and ii) creates synergistic catalytic breakdown of ethanol. Altogether, the ZnO coated TiO_2 nanotube layer demonstrated higher sensitivity, shorter response and recovery time, as well as outstanding stability and reproducibility. The present results show that the additional thin ALD ZnO coatings within anodic 1D TiO_2 nanotube layers open up new perspectives on utilization of these highly ordered nanotubular scaffolds. This novel 1D heterostructure bears

potential especially for the light-assisted applications (including photocatalytic degradation of organic dyes, solar cells) as well as various gas and chemical sensors with low operational temperature. Such heterostructure is specific for 1D nanotubular layers and cannot be achieved with nanoparticulate or mesoporous layers, for example.

4. Experimental Section

*Synthesis of self-organized TiO_2 nanotube layers***:** Titanium (Ti) foils were anodized in ethylene glycol based electrolyte containing 10 % water and 0.15 M NH_4F, 100 V at room temperature using a high-voltage potentiostat (PGU-200V, IPS Elektroniklabor GmbH) to fabricate TiO_2 nanotube layers of thicknesses ~5 μm and inner diameters ~230 nm.[46] Subsequently, the TiO_2 nanotube layers were annealed at 400 ^oC, to obtain crystalline nanotube layers in anatase phase which improves their electrical conductivity.[69]

Synthesis of reference TiO_2 mesoporous layers: Reference TiO_2 mesoporous layers were prepared from Ti Nanoxide T/SP paste (Solaronix) by spin coating on pre-annealed Ti substrates at 400 °C for 1 h (Ti with thermal oxide on the top) using spin speed 6000 rpm for 30 s. As-deposited samples were dried at 60 °C for 2 h and finally annealed at 400 °C for 1 h in a muffle furnace. The total thickness was approximately 5 μm which is comparable to the thickness of TiO_2 nanotube layers.

ALD ZnO coatings: In the next step, the TiO_2 nanotube and mesoporous layers were coated by ZnO thin films using atomic layer deposition (TFS200, Beneq). The Diethyl zinc (DEZ) (electronic grade 99.9998 %, Strem) and Millipore deionized water (18 MΩ) were used as the zinc precursor and the oxygen source, respectively, both used at temperature of 20 ^oC. High purity nitrogen (99.9999 %) was the carrier and purging gas at a flow rate of 400 standard cubic centimeters minute (sccm). Under these deposition conditions, one growth ALD cycle was defined by the following sequence: DEZ pulse (500 ms)-N_2 purge (4 s)-H_2O pulse (500

ms)-N_2 purge (5 s). The TiO_2 nanotube layers were coated by applying a different number of cycles (1, 10, 40 and 100), which led to ZnO coating nominal thicknesses of 0.19, 1.9, 7.6 and 19 nm respectively, as examined by ellipsometric measurements carried out on ZnO thin layers deposited on Si wafers, using variable angle spectroscopic ellipsometry (using VASE® ellipsometer, J.A. Woollam, Co., Inc.). All deposition processes were carried out at 200 ^{o}C. The ALD process was carried out according to the optimal conditions from the literature.[47,70]

Characterizations: The morphology of the blank and ZnO coated TiO_2 nanotube layers was characterized by a field-emission scanning electron microscope (SEM, JEOL JSM 7500F) and a scanning transmission electron microscope (STEM, FEI Tecnai F20 X-Twin) fitted with a high angle annular dark field (HAADF) detector, operated at 200 kV. The cross-sectional views were obtained from fractured samples subjected to mechanical bending. Dimensions of the blank and ZnO (100 ALD cycles) coated TiO_2 nanotube layers were measured and statistically evaluated using proprietary Nanomeasure software. Average values and standard deviations were calculated from at least 3 different locations with a high number of measurements ($n > 100$). X-ray diffraction analyses (XRD) of the ZnO coated TiO_2 nanotube layers was carried out using X-ray diffractometer (D8 Advance, Bruker AXE) using Cu Kα radiation with secondary graphite monochromator and Na(Tl)I scintillation detector. Diffuse reflectance spectra were recorded from spectral range 250 to 900 nm by UV/VIS/NIR spectrophotometer (Jasco V-570) equipped with an integrating sphere (Jasco ISN-470).

Photoelectrochemical (PEC) measurements: The photocurrent measurements were carried out in an aqueous electrolyte containing 0.1 M Na_2SO_4 employing a photoelectric spectrophotometer (Instytut Fotonowy) connected with the modular electrochemical system AUTOLAB (PGSTAT 204 Metrohm Autolab B.V.) operated with *Nova 1.10* software. A three-electrode cell with a flat quartz window was employed with a Ag/AgCl reference electrode, a Pt wire counter electrode and TiO_2 nanotube or mesoporous layers as working electrode, pressed against an O-ring of the electrochemical cell leading to an irradiated sample

area of 0.28 cm^2. Monochromatic light was provided by a 150 W Xe lamp. The photocurrents were measured in the potential range from 0.4 V to 2 V vs. Ag/AgCl (3 M KCl) with 0.4 V step in the spectral region from 305 to 500 nm with 5 nm step. The photo-transients were measured for 10 s.

Gas sensing measurements: The ethanol sensing response was evaluated in a gas test system (see **Figure S3** (Supporting Information)) that consisted of a gas cylinder filled with synthetic air, three mass flow controllers (Sierra Instruments), two glass vessels (the first with deionized water, the second with 10 ml of liquid ethanol), a test chamber, and a source-meter unit (SMU) KEITHLEY 2612B connected to a PC. Residual humidity from liquid ethanol (≥ 99.8 %) was removed by using a molecular sieve. Afterwards, it was bubbled by synthetic air (flow rate 2.4, 7.9, 11.8, 15.8 and 30 ml min^{-1}) in order to prepare ethanol vapors which were subsequently mixed with humidified synthetic air to achieve a particular concentration of gaseous ethanol (480, 810, 1020, 1170 and 1930 ppm, respectively) with defined humidity (60 %) and a total flow rate (1400 ml/min). All levels of concentration were calculated based on weight loss of liquid ethanol and correctness of the calculation was verified by a commercial ethanol gas sensor TGS 2620 (FIGARO). Tested samples were placed in the test chamber on a heating element, the temperature of which was kept at 100 or 200 °C within the whole experiment. The electrical resistance was measured by means of four-wire method (test current equaled 15 μA) every other second. The response of the sensor was defined as R_O/R_g, where R_O and R_g were the initial electrical resistance in air and the electrical resistance when targeted gas was applied, respectively.

Supporting Information

Supporting Information is available from the Wiley Online Library or from the author.

Acknowledgements

European Research Council and Ministry of Youth, Education and Sports of the Czech Republic are acknowledged for financial support of this work through projects 638857 and LM2015082, LO1607, respectively. We thank Dr. Lukáš Střižík and Mrs. Denisa Janebova for ellipsometric measurements and technical support, respectively.

Received: ((will be filled in by the editorial staff))
Revised: ((will be filled in by the editorial staff))
Published online: ((will be filled in by the editorial staff))

References

[1] M. Assefpour-Dezfuly, C. Vlachos, E. H. Andrews, *J. Mater. Sci.* **1984**, *19*, 3626.

[2] V. Zwilling, M. Aucouturier, E. Darque-Ceretti, *Electrochim. Acta* **1999**, *45*, 921.

[3] J. M. Macak, H. Tsuchiya, P. Schmuki, *Angew. Chemie Int. Ed.* **2005**, *44*, 2100; *Angew. Chem.* **2005**, *117*, 2136.

[4] J. M. Macak, H. Tsuchiya, L. Taveira, S. Aldabergerova, P. Schmuki, *Angew. Chemie Int. Ed.* **2005**, *44*, 7463; *Angew. Chem.* **2005**, *117*, 7629.

[5] J. M. Macak, H. Tsuchiya, A. Ghicov, K. Yasuda, R. Hahn, S. Bauer, P. Schmuki, *Curr. Opin. Solid State Mater. Sci.* **2007**, *11*, 3.

[6] K. Lee, A. Mazare, P. Schmuki, *Chem. Rev.* **2014**, *114*, 9385.

[7] D.-J. Yang, H. Park, S.-J. Cho, H.-G. Kim, W.-Y. Choi, *J. Phys. Chem. Solids* **2008**, *69*, 1272.

[8] P. Roy, D. Kim, K. Lee, E. Spiecker, P. Schmuki, *Nanoscale* **2010**, *2*, 45.

[9] J. M. Macak, M. Zlamal, J. Krysa, P. Schmuki, *Small* **2007**, *3*, 300.

[10] Z. Liu, X. Zhang, S. Nishimoto, T. Murakami, A. Fujishima, *Environ. Sci. Technol.* **2008**, *42*, 8547.

[11] O. K. Varghese, D. Gong, M. Paulose, K. G. Ong, C. A. Grimes, in *Sens. Actuator B - Chem.*, **2003**, pp. 338–344.

[12] P. M. Perillo, D. F. Rodríguez, *Sens. Actuator B - Chem.* **2012**, *171–172*, 639.

[13] J. Park, S. Bauer, K. Von Der Mark, P. Schmuki, *Nano Lett.* **2007**, *7*, 1686.

[14] N. K. Shrestha, J. M. Macak, F. Schmidt-Stein, R. Hahn, C. T. Mierke, B. Fabry, P. Schmuki, *Angew. Chemie Int. Ed.* **2009**, *48*, 969; *Angew. Chem.* **2009**, *121*, 987.

[15] I. M. Szilágyi, E. Santala, M. Heikkilä, V. Pore, M. Kemell, T. Nikitin, G. Teucher, T. Firkala, L. Khriachtchev, M. Räsänen, M. Ritala, M. Leskelä, *Chem. Vap. Depos.* **2013**, *19*, 149.

[16] W. Li, S. Ma, Y. Li, G. Yang, Y. Mao, J. Luo, D. Gengzang, X. Xu, S. Yan, *Sens. Actuator B - Chem.* **2015**, *211*, 392.

[17] S. Luo, F. Su, C. Liu, J. Li, R. Liu, Y. Xiao, Y. Li, X. Liu, Q. Cai, *Talanta* **2011**, *86*, 157.

[18] N. K. Shrestha, M. Yang, Y. C. Nah, I. Paramasivam, P. Schmuki, *Electrochem. Commun.* **2010**, *12*, 254.

[19] R. Lü, W. Zhou, K. Shi, Y. Yang, L. Wang, K. Pan, C. Tian, Z. Ren, H. Fu, *Nanoscale* **2013**, *5*, 8569.

[20] J. M. Macak, J. Prikryl, H. Sopha, L. Strizik, *Phys. Status Solidi - Rapid Res. Lett.* **2015**, *9*, 516.

[21] H. Cai, Q. Yang, Z. Hu, Z. Duan, Q. You, J. Sun, N. Xu, J. Wu, *Appl. Phys. Lett.* **2014**, *104*, 53114.

[22] T. G. Ulusoy, A. Ghobadi, A. K. Okyay, *J. Mater. Chem. A* **2014**, *2*, 16867.

[23] E. García-Ramírez, M. Mondragón-Chaparro, O. Zelaya-Angel, *Appl. Phys. A* **2012**, *108*, 291.

[24] M. I. Khan, K. A. Bhatti, R. Qindeel, L. G. Bousiakou, N. Alonizan, Fazal-e-Aleem, *Results Phys.* **2016**, *6*, 156.

[25] M. M. Momeni, Y. Ghayeb, *J. Appl. Electrochem.* **2015**, *45*, 557.

[26] A. Sarkar, A. K. Singh, G. G. Khan, D. Sarkar, K. Mandal, *RSC Adv.* **2014**, *4*, 55629.

[27] M. Kwiatkowski, I. Bezverkhyy, M. Skompska, *J. Mater. Chem. A* **2015**, *3*, 12748.

[28] S. Hernández, V. Cauda, D. Hidalgo, V. Farías Rivera, D. Manfredi, A. Chiodoni, F. C. Pirri, *J. Alloys Compd.* **2014**, *615*, S530.

[29] X. Yan, C. Zou, X. Gao, W. Gao, *J. Mater. Chem.* **2012**, *22*, 5629.

[30] S. Hernández, V. Cauda, A. Chiodoni, S. Dallorto, A. Sacco, D. Hidalgo, E. Celasco, C. F. Pirri, *ACS Appl. Mater. Interfaces* **2014**, *6*, 12153.

[31] G. S. Pozan, A. Kambur, *Chemosphere* **2014**, *105*, 152.

[32] D. Chen, H. Zhang, S. Hu, J. Li, *J. Phys. Chem. C* **2008**, *112*, 117.

[33] C. Cheng, A. Amini, C. Zhu, Z. Xu, H. Song, N. Wang, *Sci. Rep.* **2014**, *4*, 4181.

[34] A. Ghobadi, T. G. Ulusoy, R. Garifullin, M. O. Guler, A. K. Okyay, *Sci. Rep.* **2016**, *6*, 30587.

[35] J. Deng, B. Yu, Z. Lou, L. Wang, R. Wang, T. Zhang, *Sens. Actuator B - Chem.* **2013**, *184*, 21.

[36] S. Park, S. An, H. Ko, S. Lee, H. W. Kim, C. Lee, *Appl. Phys. A Mater. Sci. Process.* **2014**, *115*, 1223.

[37] A. Katoch, J.-H. Kim, S. S. Kim, *ACS Appl. Mater. Interfaces* **2014**, *6*, 21494.

[38] S. Yuan, J. Mu, R. Mao, Y. Li, Q. Zhang, H. Wang, *ACS Appl. Mater. Interfaces* **2014**, *6*, 5719.

[39] M. Leskelä, M. Ritala, *Angew. Chemie Int. Ed.* **2003**, *42*, 5548; *Angew. Chem.* **2003**, *115*, 5706.

[40] H. Cai, P. Liang, Z. Hu, L. Shi, X. Yang, J. Sun, N. Xu, J. Wu, *Nanoscale Res. Lett.* **2016**, *11*, 104.

[41] R. Zazpe, M. Knaut, H. Sopha, L. Hromadko, M. Albert, J. Prikryl, V. Gärtnerová, J. W. Bartha, J. M. Macak, *Langmuir* **2016**, *32*, 10551.

[42] R. Zazpe, J. Prikryl, V. Gärtnerova, K. Nechvilova, L. Benes, L. Strizik, A. Jäger, M. Bosund, H. Sopha, J. M. Macak, *Langmuir* **2017**, *33*, 3208.

[43] H. Sopha, G. D. Salian, R. Zazpe, J. Prikryl, L. Hromadko, T. Djenizian, J. M. Macak,

ACS Omega **2017**, *2*, 2749.

[44] H. Sopha, M. Krbal, S. Ng, J. Prikryl, R. Zazpe, F. K. Yam, J. M. Macak, *Appl. Mater. Today* **2017**, *9*, 104.

[45] M. Krbal, J. Prikryl, R. Zazpe, H. Sopha, J. M. Macak, *Nanoscale* **2017**, *9*, 7755.

[46] S. Das, H. Sopha, M. Krbal, R. Zazpe, V. Podzemna, J. Prikryl, J. M. Macak, *ChemElectroChem* **2017**, *4*, 495.

[47] V. Rogé, N. Bahlawane, G. Lamblin, I. Fechete, F. Garin, A. Dinia, D. Lenoble, *J. Mater. Chem. A* **2015**, *3*, 11453.

[48] R. Beranek, H. Tsuchiya, T. Sugishima, J. M. Macak, L. Taveira, S. Fujimoto, H. Kisch, P. Schmuki, *Appl. Phys. Lett.* **2005**, *87*, 243114.

[49] H. Tsuchiya, J. M. Macak, A. Ghicov, A. S. Räder, L. Taveira, P. Schmuki, *Corros. Sci.* **2007**, *49*, 203.

[50] J. M. Macak, A. Ghicov, R. Hahn, H. Tsuchiya, P. Schmuki, *J. Mater. Res.* **2006**, *21*, 2824.

[51] J. Bao, I. Shalish, Z. Su, R. Gurwitz, F. Capasso, X. Wang, Z. Ren, *Nanoscale Res. Lett.* **2011**, *6*, 404.

[52] K. G. Saw, S. S. Tneh, F. K. Yam, S. S. Ng, Z. Hassan, *PLoS One* **2014**, *9*, 1.

[53] R. S. Mane, W. J. Lee, H. M. Pathan, S.-H. Han, *J. Phys. Chem. B* **2005**, *109*, 24254.

[54] C. C. Li, Z. F. Du, L. M. Li, H. C. Yu, Q. Wan, T. H. Wang, *Appl. Phys. Lett.* **2007**, *91*, 1.

[55] P. Hu, G. Du, W. Zhou, J. Cui, J. Lin, H. Liu, D. Liu, J. Wang, S. Chen, *ACS Appl. Mater. Interfaces* **2010**, *2*, 3263.

[56] Z. Zhao, D. Wang, X. Kang, Y. Sang, H. Liu, *Energy Environ. Focus* **2014**, *3*, 404.

[57] Y. Wang, Z. Yun, C. Meng, Z. Gao, X. Cao, X. Li, L. Xu, W. Zhu, X. Peng, B. Zhang, Y. Lin, L. Liu, *Nanotechnology* **2016**, *27*, 425503.

[58] D. Ju, H. Xu, J. Zhang, J. Guo, B. Cao, *Sens. Actuator B - Chem.* **2014**, *201*, 444.

[59] T. Jinkawa, G. Sakai, J. Tamaki, N. Miura, N. Yamazoe, *J. Mol. Catal. A Chem.* **2000**, *155*, 193.

[60] B. L. Zhu, C. S. Xie, W. Y. Wang, K. J. Huang, J. H. Hu, *Mater. Lett.* **2004**, *58*, 624.

[61] R. Uma, J. C. Kuriacose, *Proc. Indian Natl. Sci. Acad.* **1975**, *41*, 36.

[62] D. R. Miller, S. A. Akbar, P. A. Morris, *Sens. Actuator B - Chem.* **2014**, *204*, 250.

[63] A. J. T. Naik, I. P. Parkin, R. Binions, *IEEE Sens. J.* **2014**, *14*, 3137.

[64] A. Naik, I. Parkin, R. Binions, *Chemosensors* **2016**, *4*, 3.

[65] T. Tharsika, A. S. M. A. Haseeb, S. A. Akbar, M. Faizul, M. Sabri, W. Y. Hoong, *Sensors* **2014**, *14*, 14586.

[66] Y. Wang, L. Liu, C. Meng, Y. Zhou, Z. Gao, X. Li, X. Cao, L. Xu, W. Zhu, *Sci. Rep.* **2016**, *6*, 33092.

[67] B. G. Streetman, S. K. Banarjee, *Solid State Electronic Devices*, Prentice Hall, **2009**.

[68] C. Jin, S. Park, H. Kim, C. Lee, *Sens. Actuator B - Chem.* **2012**, *161*, 223.

[69] S. Das, R. Zazpe, J. Prikryl, P. Knotek, M. Krbal, H. Sopha, V. Podzemna, J. M. Macak, *Electrochim. Acta* **2016**, *213*, 452.

[70] E. Guziewicz, M. Godlewski, L. Wachnicki, T. A. Krajewski, G. Luka, S. Gieraltowska, R. Jakiela, A. Stonert, W. Lisowski, M. Krawczyk, J. W. Sobczak, A. Jablonski, *Semicond. Sci. Technol.* **2012**, *27*, 74011.

The table of contents:

Ultrathin and homogeneous ZnO coatings within high aspect ratio TiO_2 nanotubular structure. ALD ZnO coatings within high surface area TiO_2 nanotubes layer form a heterojunction with excellent photoelectrochemical activity and good ethanol sensing response. These enhancements are contributed by the passivated surface traps on tube wall, increased light absorption, close match of coating thickness and Debye length.

Keywords: self-organized TiO_2 nanotubes, ZnO coatings, ALD, charge separation, ethanol sensing

S.W. Ng, P. Kuberský, M. Krbal, J. Prikryl, V. Gärtnerová, D. Moravcová, H. Sopha, R. Zazpe, F. K. Yam, A. Jäger, L. Hromádko, L. Beneš, A. Hamáček and J. M. Macak*

ZnO Coated Anodic 1D TiO_2 Nanotube Layers: Efficient Photo-electrochemical and Gas Sensing Heterojunction

ToC figure

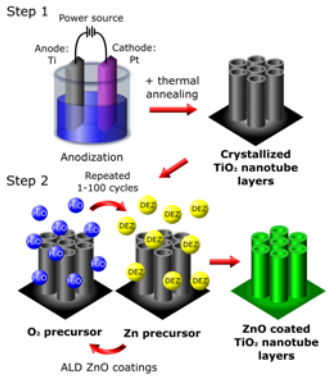

Supporting Information

ZnO Coated Anodic 1D TiO_2 Nanotube Layers: Efficient Photo-electrochemical and Gas Sensing Heterojunction

*Siowwoon Ng, Petr Kuberský, Milos Krbal, Jan Prikryl, Viera Gärtnerová, Daniela Moravcová, Hanna Sopha, Raul Zazpe, Fong Kwong Yam, Aleš Jäger, Luděk Hromádko, Ludvík Beneš, Aleš Hamáček and Jan M. Macak**

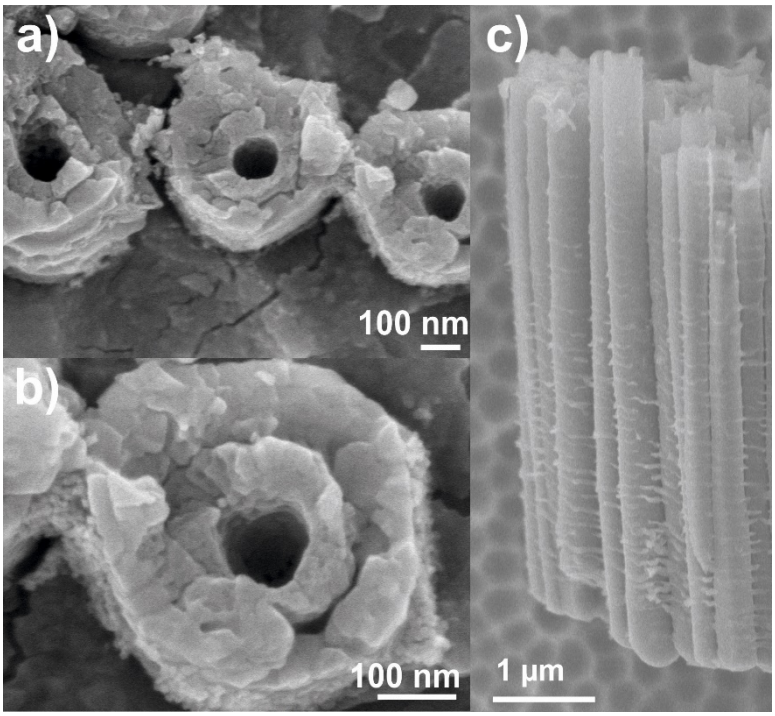

Figure S1. (a,b) SEM images of the nanotube parts of TiO_2 nanotube layers close to the interface with Ti substrates, (c) Cross sectional SEM image that reveals the nanotube layers thickness of approximately 5 µm.

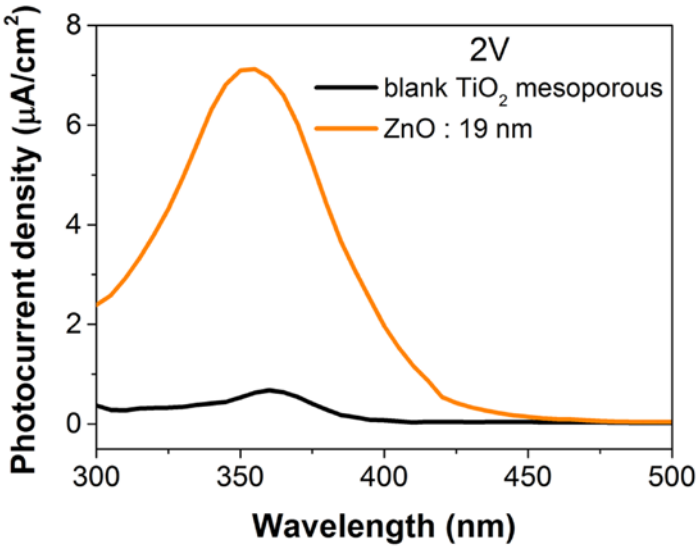

Figure S2. Photocurrent densities for blank and ZnO coated (19 nm) TiO_2 mesoporous layers, measured at 2 V.

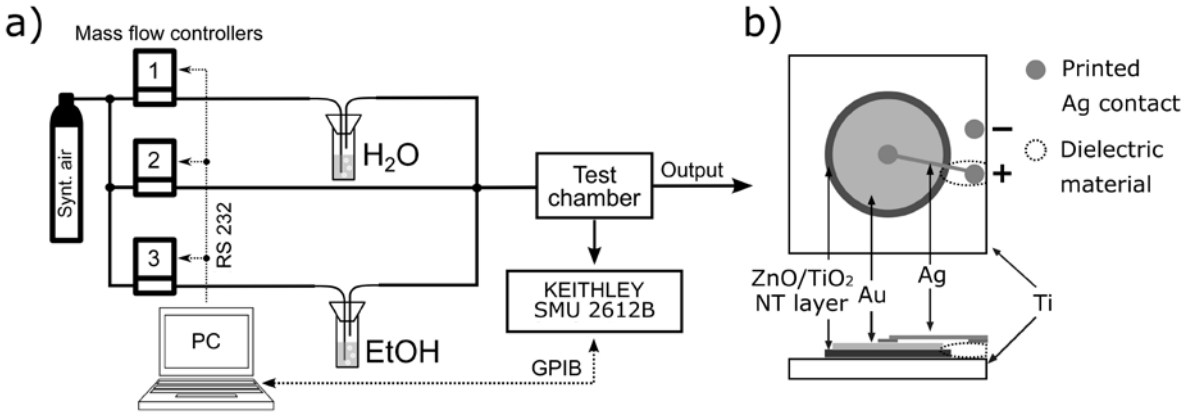

Figure S3. Schematic diagram of the (a) gas sensing setup for ethanol sensing response measurement, (b) gas sensor structure: top and side view.

Table S1. Thicknesses of walls of TiO_2 nanotube layers and ZnO coating (nominally 19 nm–thick = 100 ALD cycles), measured at top, middle and bottom of the tube layers.

	Top tube wall thickness (nm)	**Middle tube wall thickness (nm)**	**Bottom tube wall thickness (nm)**
TiO_2 nanotube layers	56.7 ± 6.9	94.6 ± 21.7	127.8 ± 12.4
	Top tube coating thickness (nm)	**Middle tube coating thickness (nm)**	**Bottom tube coating thickness (nm)**
ZnO coating (19 nm thickness)	18.7 ± 1.8	18.1 ± 1.7	17.9 ± 1.4